Frequency Dependency of Measured Highly Resolved Directional Propagation Channel Characteristics

Invited paper

Jonas Medbo, Nima Seifi, and Henrik Asplund
Ericsson Research, SE-164 80 Stockholm, Sweden
Email: forename.surname@ericsson.com

***Abstract*— An indoor measurement campaign has been conducted in order to determine any frequency dependent characteristics of the directional radio propagation channel over the frequency range 6-60 GHz. For the analysis a novel method, which previously has been proven to provide exceptional measurement accuracy at 58.7 GHz, is used. Herein it is shown that the measured channel power distributions over direction and delay are surprisingly similar over the full frequency range in both LOS and NLOS conditions. One exception is that the window transmission attenuation and reflectivity is substantially different at the two frequencies 5.8 GHz and 14.8 GHz. This difference results in that one of two dominant pathways at 14.8 GHz goes out of the building and is reflected off an adjacent building back in again to the receiver location. This does not occur at 5.8 GHz as the windows block penetration at this frequency.**

I. INTRODUCTION

The main purpose of this paper is to support the channel modelling efforts for the fifth generation (5G) cellular networks [1]-[2] by providing solid experimental basis of important radio channel characteristics over the frequency range 6-60 GHz. This study focuses on the frequency dependency of highly resolved channel characteristics in the angle and delay domains. As pointed out in [3]-[4], super resolution methods for estimating these characteristics may provide biased results depending on corresponding model assumptions. In particular the so called diffuse component may not be reliably characterised. A commonly used method to directly measure the directional channel characteristics is to scan different ranges of space angle by means of directive antennas combined with rotation modules [5]-[9]. This method does not suffer from bias due to model assumptions. However, the method is limited by antenna pattern side lobe levels. The novel method presented and validated in [12] does not suffer from any of these problems as it is based on standard beamforming optimized to suppress side lobes more than 50 dB over the full space angle. This novel method is based on massive sampling of the channel in 3D space using a single antenna element. Off-line FFT methods are then used to provide both angle and delay information. Due to this method's high resolution and small bias it is chosen for the analysis presented herein.

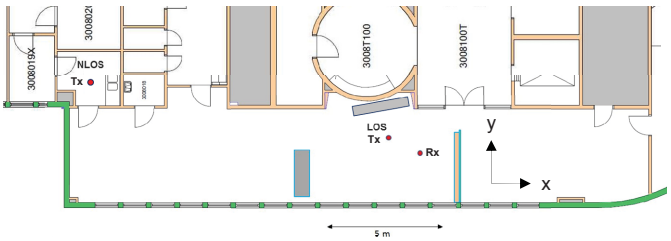

Fig. 1. Measurement scenario. The Tx antenna was placed close to the Rx antenna in the LOS measurements, and, in a small kitchen in the end of the office space in the NLOS measurements.

II. MEASUREMENTS

The measurements were performed in an indoor office environment both in line of sight (LOS) and non-line of sight (NLOS) conditions (see Fig. 1). Vertical half-wave dipole antennas (2 dBi), at 1.5 m height above the floor level, were used both at the transmitter (Tx) and the receiver (Rx) in all measurements. Three carrier frequencies were used at 5.8 GHz, 14.8 GHz and 58.7 GHz with bandwidths of 150 MHz, 200 MHz, and 2 GHz, respectively. A short link distance of 1.5 m was used for the LOS measurement. For the NLOS measurements, the Rx antenna was placed in a small kitchen at the end of the office space (see Fig. 1). The distance between the Tx and the Rx antennas in the NLOS case was 14 m. It should be noted that the NLOS scenario was measured only at 5.8 GHz and 14.8 GHz due to that the access to the indoor environment was ended in the middle of the campaign.

The frequency response of the radio propagation channel was measured by means of a vector network analyzer (VNA) using 1601 frequency samples. To provide high resolution directional measurement results the channel was sampled massively in space (commonly referred to as the virtual antenna method). For this purpose an antenna positioning robot was used for sampling the channel at Rx in cubic space volume of about ten wavelengths size. The number of samples in each dimension is 25 resulting in a total number of 25x25x25=15625 space samples which is an extreme number even for the virtual antenna method. The corresponding cube sizes at 5.8 GHz, 14.8 GHz, and 58.7 GHz, were 48 cm, 19.2 cm and 4.8 cm respectively. The virtual antenna array method has commonly been used at sub millimeter wavelengths previously [10]. It has also successfully been used at 60 GHz

ISBN 978-3-8007-4221-9

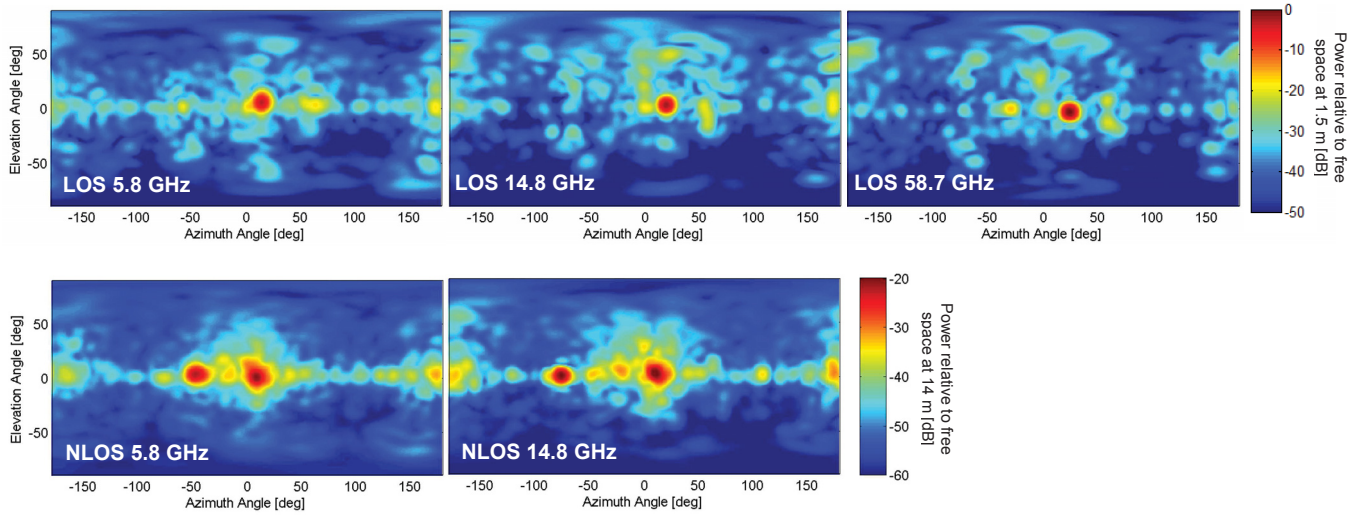

Fig. 2. Measured directional power spectra. Here, zero degrees in azimuth correspond to the negative x direction in Fig. 1.

in an indoor MIMO measurement campaign [11]. However, no previous results providing simultaneous high angular resolution, full space angle characterization, and, more than 50 dB side-lobe suppression have been found in literature except [12].

III. Analysis Method

In order to provide comparable characteristic over all measured frequencies the measurement data need some adjustment prior to analysis. For this purpose the measurement bandwidths are equalized in the analysis, meaning that the 14.8 GHz and the 58.7 GHz measurement data are reduced to the bandwidth of the 5.8 GHz measurement data of 150 MHz. This equalization is important to avoid that strong specular spikes might dominate power delay profiles at higher frequencies due to that much larger bandwidth is available. The height of any specular (or LOS) peak of the power delay profile is actually proportional to the measurement bandwidth while the non-resolved diffuse part stays constant. Furthermore, the measurements at 58.7 GHz are affected by attenuation due to oxygen absorption. In order to provide results suitable for frequency consistent channel modelling and interpolation, this attenuation is removed in the analysis by compensating the power delay profiles with 1.5 dB/m propagation distance at this frequency.

The directional analysis is based on straight forward beamforming. Due to the computational challenge to process the huge size of data for each measured channel fast Fourier transformation (FFT) is used both for transformation from space (3D) to direction domain and from frequency to delay domain. In both cases Hanning windowing is used for suppression of the side-lobes.

The 3D space samples of the channel are transformed to 3D wave vector domain using FFT. It should be noted that the only physical possible values of the wave vector $\mathbf{k}$ lie on a sphere fulfilling

$$|\mathbf{k}| = \frac{2\pi}{\lambda} \quad (1)$$

where λ is the wavelength. As the wave vector $\mathbf{k}$ determines the direction of each wave the directional channel response is obtained by interpolating desired azimuth angles, [-180°,180°], and elevation angles, [-90°,90°], on this sphere. For the virtual antenna array size used herein an angular resolution of 8 degrees (half power beamwidth) is provided. More details about this method, including performance evaluation, are provided in [12].

IV. Results

In this section the results of analysed measurement data are presented. The focus is put on comparing key characteristics at the different frequencies.

A. Directional Power Spectra

The directional power spectra of the measured channels shown in Fig. 2 were obtained by summing the power in the delay domain. In the LOS graphs the power has been normalized to the free space power at 1.5 m distance which was the distance of the 58.7 GHz measurement. As the measurements were performed at different occasions, the link distance of the 5.8 GHz and 14.8 GHz measurements was somewhat larger (2 m) explaining why the LOS peak in the centre is somewhat weaker at those frequencies. Though the measurements at the different frequencies were performed at different occasions with slightly different placements of antennas (c.f. the LOS direction which differ slightly in the graphs) the directional power spectra are strikingly similar for all frequencies. One small frequency dependent difference is observed in the LOS graphs where a band of higher signal power around zero degrees elevation angle is most pronounced at 5.8 GHz and least pronounced at 14.8 GHz. This difference is explained by that the reflectivity of the windows was found out to be substantially higher at 5.8 GHz than at the other frequencies.

ISBN 978-3-8007-4221-9

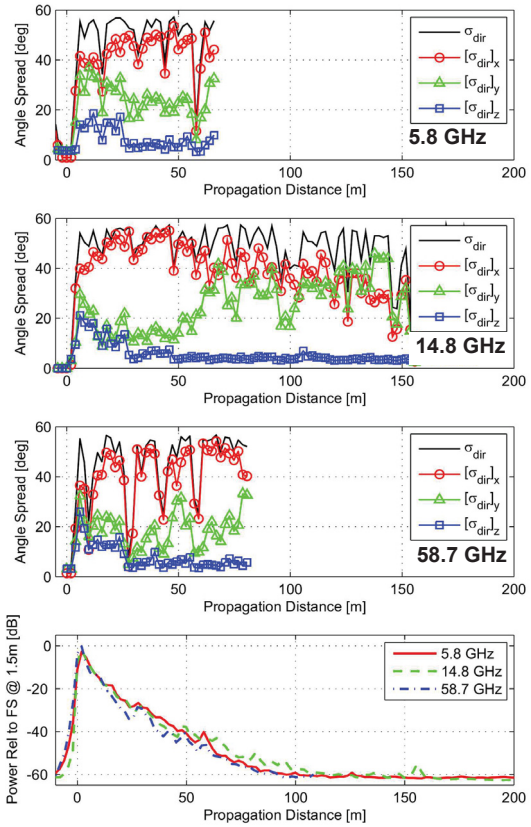

Fig. 3. Measured directional spread versus propagation distance ($d = \tau \cdot c$) for the LOS scenario and the three different frequencies (three upper) and corresponding power propagation distance profiles (lower). The power propagation distance profiles are normalized to the free space power at 1.5 m.

The NLOS graphs differ from the LOS graphs in that the diffuse cluster around the main peak is more focused and that there are not one but a few strong directions. Further, the received power is attenuated about 20 dB relative to free space propagation for the link distance of 14 m. The graphs of the two measured frequencies remain strikingly similar, as in the LOS case. One observed difference is the peak at -50 degrees in azimuth which is strong at 5.8 GHz and weak at 14.8 GHz. The opposite effect is observed for the peak at -75 degrees in azimuth where the power is strong at 14.8 GHz and weak at 5.8 GHz. This is again the effect of frequency dependent window attenuation/reflection.

B. Directional Spread

As pointed out in our previous study [12], common directional spread measures like ordinary r.m.s. azimuth and elevation spread are problematic when the full space angle is analyzed. The problem is that ordinary azimuth and elevation spread are both cyclic and non-Euclidian and are not well defined at the poles. In this study the following directional spread measure [13] is therefore used instead

$$\sigma_{dir} = \frac{180}{\pi}\sqrt{\int\left|\hat{\mathbf{u}} - \boldsymbol{\mu}_{\hat{\mathbf{u}}}\right|^2 P(\hat{\mathbf{u}})\,d\Omega} \quad \text{[deg]}, \tag{2}$$

where the directional power function is normalized as

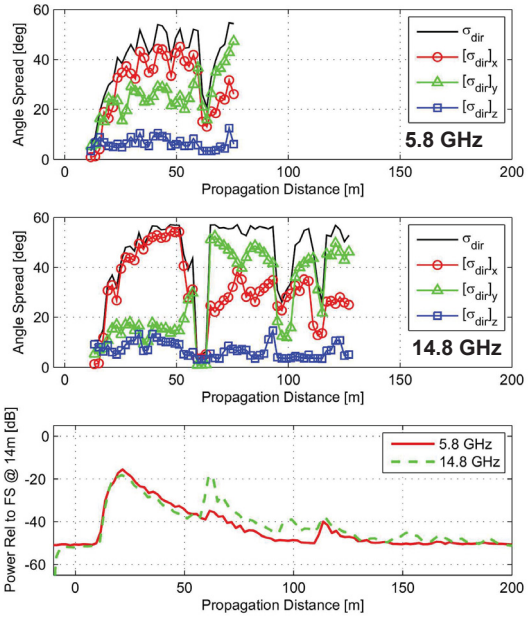

Fig. 4. Same as Fig. 3 but for the NLOS scenario. The power propagation distance profiles are normalized to the free space power at 14 m.

$$\int P(\hat{\mathbf{u}})\,d\Omega = 1$$

and

$$\boldsymbol{\mu}_{\hat{\mathbf{u}}} = \int \hat{\mathbf{u}} P(\hat{\mathbf{u}})\,d\Omega, \tag{4}$$

where $\hat{\mathbf{u}}$ is the direction unit vector. The spread may be determined for each of the three Euclidian components of $\hat{\mathbf{u}}$ (x,y,z) by

$$\left[\sigma_{dir}\right]_n = \frac{180}{\pi}\sqrt{\int\left[\hat{\mathbf{u}} - \boldsymbol{\mu}_{\hat{\mathbf{u}}}\right]_n^2 P(\hat{\mathbf{u}})\,d\Omega} \quad \text{[deg]}, \; n = \text{x,y,z}. \tag{5}$$

In order to provide comparability with ordinary azimuth and elevation spread the factor $180/\pi$ has been added to the expression used in [4]. The result is that small values of σ_{dir} correspond to ordinary r.m.s. angle spread with $\left[\sigma_{dir}\right]_x$ and $\left[\sigma_{dir}\right]_y$ representing azimuth and $\left[\sigma_{dir}\right]_z$ representing elevation. Further, σ_{dir} is by its definition upper bounded at 57.3°.

In the following analysis the, for time domain, commonly used delay, τ, is replaced with corresponding propagation distance, i.e. $d = \tau \cdot c$, in order to facilitate understanding of the distance to scattering objects. This means that the power delay profiles are replaced with power propagation distance profiles (PPDP).

In Fig. 3 the directional spreads for the LOS scenario versus propagation distance together with corresponding PPDPs are shown. Again it is striking how similar the profiles for the different frequencies are. The directional spread is shown only for the part of the PPDPs for which there is sufficient signal above the noise floor. Basically the same characteristic are

ISBN 978-3-8007-4221-9

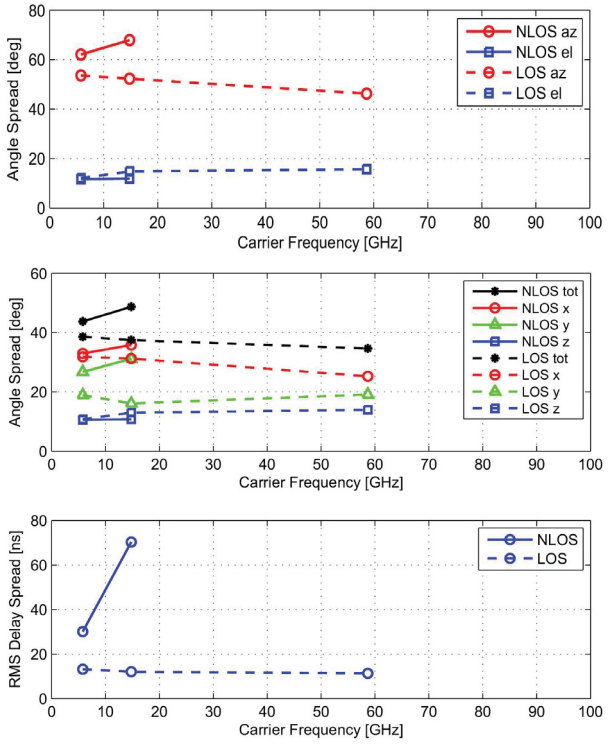

Fig. 5. Total directional spreads (upper two) and delay spreads (lower) versus carrier frequency for the different measurement scenarios. The upper plot show ordinary r.m.s. azimuth and elevation spreads while the middle show directional spreads according to the new improved definition according to equations (2)-(5)

observed at all frequencies. For the LOS spike the spread is small, around 5 degrees. At other delays the spread is typically saturated at 57.3 degrees. At a few delays where strong reflections occur the directional spread goes down. Another striking observation is that the elevation spread $\left[\sigma_{dir}\right]_z$ decays fast to very small values. For longer delays the directional spread in the x dimension $\left[\sigma_{dir}\right]_x$ dominates. Except for short delays the directional spreads in the different dimensions seem to be proportional to the corresponding lengths of the room. A likely explanation is that the power decays faster for smaller room dimensions, due to more frequent interactions with corresponding walls, floor and ceiling, resulting in smaller directional spread in those dimensions.

In Fig. 4 the corresponding graphs are shown for the NLOS scenario. The characteristics are very similar with those of the LOS scenario. One of the main observations is that there is a strong echo around 60 m propagation distance at 14.8 GHz which is not observed at 5.8 GHz. The reason for the difference is that the windows reflect/attenuate differently for different frequencies. This is an effect of the three layers of glass (non-metalized) in the windows of the room. Due to multiple reflections between these layers different frequencies are attenuated differently when transmitted through the windows. Dedicated window attenuation measurements, performed in conjunction with the channel measurements,

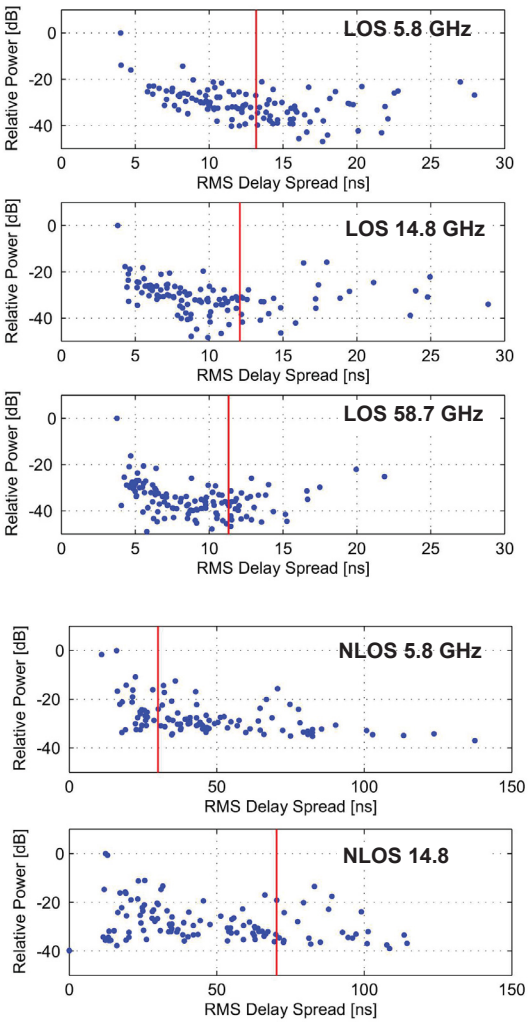

Fig. 6. Beam power versus r.m.s. delay spread distributions for the different measurements. The mean delay spread values are indicted with solid lines.

show that the window attenuation at 14.8 GHz is negligible while it is around 10 dB at 5.8 GHz. Assuming that the strong echo at 14.8 GHz is due to a pathway going out through a window reflected off a neighboring building and in again through another window explains exactly the power difference of about 20 dB (relative to 5.8 GHz) which is twice the window attenuation at 5.8 GHz. It also explains why the directional spread in the y direction increases at delays after that the radio wave corresponding to the same path has entered the room as the power of waves propagating along the y dimension of the room then is increased.

The total directional spreads, corresponding to summing the power of all delays (using angular distributions shown Fig. 2), are shown in Fig. 5 versus frequency for assessment of any frequency dependencies. Due to the shorter LOS link distance at 58.7 GHz (1.5 m) the relatively stronger LOS peak introduces a corresponding bias in directional spread (smaller spread) as compared with 5.8 and 14.8 GHz. In order to remove this bias the LOS peak has been decreased by 2.5 dB

ISBN 978-3-8007-4221-9

at 58.7 GHz in the analysis. No obvious frequency trend is observed. The trend is very similar for all scenarios where the elevation spread is small around 10 degrees and the directional spreads in x- and y-dimensions are substantially larger between 20 and 40 degrees. Moreover, the directional spread in the y-dimension is substantially larger for the NLOS scenario due to the pathway which goes out of the building and in again after reflecting off the adjacent building at 14.8 GHz and due to a strong window reflection at 5.8 GHz.

C. *Delay Spread*

The total delay spreads obtained from the profiles of Figs. 3 and 4 (i.e. by summing the power of all directions) are shown in Fig. 5. As was done in the directional spread analysis the LOS peak of the 58.7 GHz profile has been reduced by 2.5 dB also in this analysis. Again there is no obvious frequency trend. For the NLOS curve the delay spread is substantially larger at 14.8 GHz than at 5.8 GHz, but this is fully explained by the window attenuation which by occasion is very large at 5.8 GHz and very low at 14.8 GHz resulting in a very strong echo having a large delay only at 14.8 GHz (See Fig. 4).

As beamforming is expected to be an important technology component of future radio access, particularly for millimetre waves, it is important analyse delay spreads corresponding to strong directions. This analysis has been performed for the peaks in the angle power distributions (shown in Fig. 2) using a dynamic range of 30 dB for corresponding PPDPs. In Fig. 6 are shown the distributions of delay spread values for the peaks of the graphs in Fig 2. It is clear that the delay spread is very small for the one or two strongest peaks. However, for the rest of the directions the delay spreads are quite uniformly distributed and it is quite likely that a random direction results in larger delay spread than the average. This means that one cannot take for granted that delay spread goes down when directional antennas are used.

D. *Multipath Components*

Typically propagation channels are modelled by a set of discrete multipath components (MPCs). It is likely that it is possible to approximate the measured channels herein by corresponding peaks in delay and angle as they are highly resolved in both angle and delay. This has been done by identifying a MPC for each peak of each four dimensional measured channel data (3D in space + 1D in delay). In Fig. 7 the angle power distributions of the synthetized channel, using 400 MPCs, and the measured channel for the 14.8 GHz LOS scenario are shown. It is clear that the main characteristics are equal. Only the diffuse low power background is partly missing for the synthetized channel. Further the power ordered distributions of the MPCs are shown. These distributions are very similar for all frequencies. A clear difference between the LOS and NLOS scenarios is however observed. There is a single dominating MPC in LOS whereas the distribution is more uniform in NLOS. This effect is also seen in the cumulative power distributions as the LOS MPCs account for

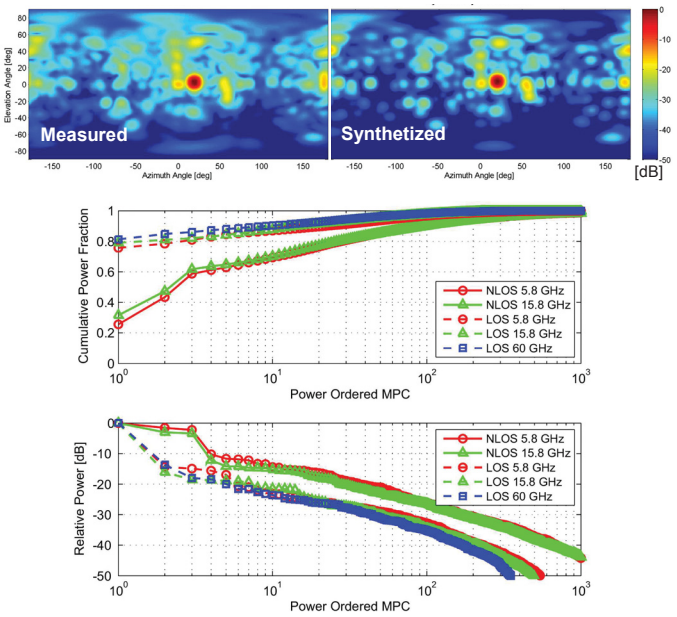

Fig. 7. Angular power distributions of measured channel and MPC based synthetized channel for the 14.8 GHz LOS scenario (upper) and corresponding power ordered distributions of MPCs power and cumulative power fraction of MPCs.

around 80% of the total received power. In order to account for more than 95% of the power around 400 MPCs are sufficient for all measured channels. It should however be noted that the number of MPCs which is required to account for a specific fraction of the channel power is expected to depend on the bandwidth and angular resolution of the measurement data. The lower the bandwidth is the lower the number of required MPCs is required to account for a specific power fraction.

E. *Scattering Objects*

In order to get some insight on the radio wave scattering properties of the environment, the measured directional power distributions have been put on top of a panoramic photograph taken from the virtual antenna array location, as was done in the previous 60 GHz analysis [12]. This is shown in Fig. 8 for NLOS at 5.8 GHz and 14.8 GHz. The LOS graphs are not shown as the corresponding characteristics are very similar for all frequencies and detailed results for 58.7 GHz are presented in [12].

It is clear that the results are very similar for the two frequencies. The main direction is close to the door opening to the kitchen where the Tx is located (See Fig. 1). Further there seems to be some significant scatterers in the ceiling. There are clear reflections off the walls and the windows. In the 5.8 GHz plot there is also one strong window reflection. The reason for such a strong window reflection is that the window reflectivity is high at 5.8 GHz. For 14.8 GHz, however, this reflection seems to be much weaker which is attributed to low window reflectivity at this frequency. There is however a dominant peak from a window further to the left at 14.8 GHz.

ISBN 978-3-8007-4221-9

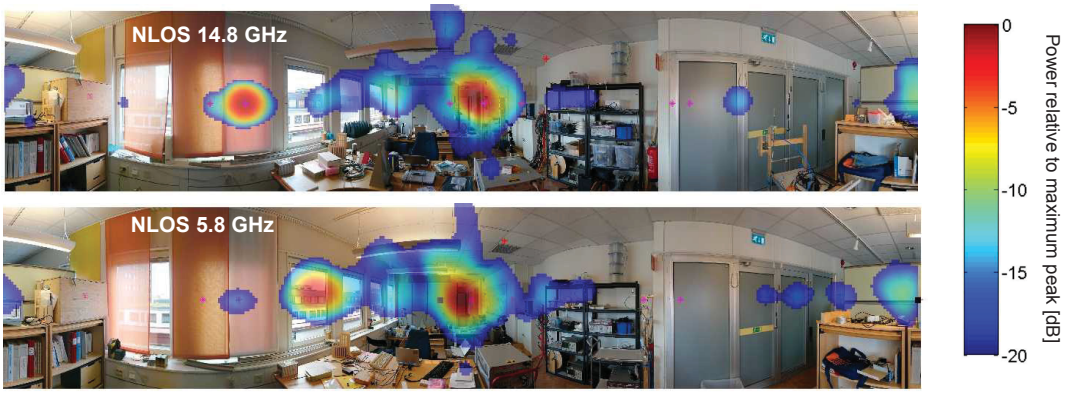

Fig. 8. Directional power distribution on panoramic photograph from the Rx location.

The reason is that the corresponding wave has propagated out of the building and back in again reflected off the adjacent building across the street. This peak is also observed at 5.8 GHz substantially more attenuated. The difference is explained by the fact that the window transmission loss is substantial at 5.8 GHz while it is negligible at 14.8 GHz as explained it the previous section.

V. Conclusions and Discussion

The main goal of this work is to improve the understanding of the frequency dependency of highly resolved directional radio channels. For this purpose measured channels at 5.8 GHz, 14.8 GHz and 58.7 GHz in an indoor scenario in both LOS and NLOS have been compared. The observed channel characteristics are generally very similar at all frequencies. The only clear difference which is observed is due to that the window attenuation by occasion is large at 5.8 GHz and negligible at 14.8 GHz. The phenomenon is due to constructive and destructive interference by reflections between the three glass layers of the windows. Moreover, the angle spread is concentrated in the long horizontal extension of the room where the virtual measurement antenna array was located. The spread in elevation is minor except for very small delays when the link distance is small. Each distinct spike in the power delay profile is characterized by small angle spread in all spatial dimensions (x,y,z). Between the peaks of the power delay profile, substantial angle spread is observed in the horizontal plane (x,y).

The main finding of this study is that both the directional and the delay properties of the measured radio channel in the range 6-60 GHz basically seem to be frequency independent for the specific indoor environment studied. This is a very positive result as it indicates that 5G channel modelling for the indoor office scenario could be simplified in that no frequency dependency needs to be assumed.

Acknowledgment

The research leading to these results received funding from the European Commission H2020 programme under grant agreement no. 671650 (mmMAGIC project). The authors would like to acknowledge the contributions of their colleagues in mmMAGIC, although the views expressed are those of the authors and do not necessarily represent the project. Further the authors would like to acknowledge Martin Furuskog who actually performed all measurements except the one at 58.7 GHz.

References

[1] ITU-R M.2083, “Framework and overall objectives of the future development of IMT for 2020 and beyond,” Sep. 2015.
[2] 3GPP TR 38.913, “Scenarios and Requirements for Next Generation Access Technologies,” V0.2.0, Feb. 2016.
[3] W. T. Kotterman, M. Landmann, G. Sommerkorn, and R. Thomä, ”On diffuse and non-resolved multipath components in directional channel characterisation”, *XXVIIIth General Assembly of URSI*
[4] F. Quitin, C. Oestges, F. Horlin, and P. De Doncker, ”Diffuse multipath component characterization for indoor MIMO channels,” *EuCAP* 2010
[5] Karttunen, A., Haneda, K., Jarvelainen, J., Putkonen, J. “Polarisation characteristics of propagation paths in indoor 70 GHz channe,” EuCAP 2015
[6] Koymen, O. H., Partyka, A., Subramanian, S., & Li, J. “Indoor mm-Wave Channel Measurements: Comparative Study of 2.9 GHz and 29 GHz,” GLOBECOM 2015
[7] D. Dupleich, S. Hafner, C. Schneider, R. Muller, R. Thoma, J. Luo, G. Wang, “Double-directional and dual-polarimetric indoor measurements at 70 GHz”, in proc. PIMRC, Hong Kong, China, Aug. 2015
[8] Deng, S., Samimi, M. K., & Rappaport, T. S. (2015, June). 28 GHz and 73 GHz millimeter-wave indoor propagation measurements and path loss models,” ICCW 2015
[9] Kim, M. D., Liang, J., Kwon, H. K., & Lee, J. (2015, August). “Directional delay spread characteristics based on indoor channel measurements at 28GHz”, PIMRC 2015
[10] Medbo, J., Asplund, H., Berg, J. E., & Jalden, N. (2012, March). “Directional channel characteristics in elevation and azimuth at an urban macrocell base station,” EUCAP 2012
[11] Gustafson, Carl, Fredrik Tufvesson, Shurjeel Wyne, Katsuyuki Haneda, and Andreas F. Molisch "Directional analysis of measured 60 GHz indoor radio channels using SAGE," VTC Spring, 2011
[12] J. Medbo, H. Asplund, J. E. Berg, ”60 GHz Channel Directional Characterization using Extreme Size Virtual Antenna Array”, in proc. PIMRC, Hong Kong, China, Aug. 2015
[13] B. H. Fleury,"First-and second-order characterization of direction dispersion and space selectivity in the radio channel." *IEEE Transactions on Information Theory*, 2000.

